ELSEVIER

*Polymer* Vol. 37 No. 9, pp. 1621–1627, 1996

0032-3861/96/$15.00+0.00

# Computer simulation of curved crystal habits: polymer crystallization under an anisotropic growth condition

**Yasutoshi Tanzawa***
*Department of Systems Engineering, Nagoya Institute of Technology, Showa-ku, Gokiso-cho, Nagoya 466, Japan*

**and Akihiko Toda†**
*Department of Physics, Faculty of Science, Kyoto University, Kyoto 606, Japan*
*(Received 28 August 1995; revised 18 October 1995)*

Computer simulation was carried out to study the morphological change in the lateral habit of polyethylene single crystals grown from the melt. Monte Carlo simulation was utilized for modelling the processes of surface nucleation and step propagation on the growth faces of a two-dimensional crystal with hexagonal packing. Anisotropy of growth was introduced in the simulation by choosing different rates for these processes on the {110} and {100} faces. Depending on the ratio of the step propagation velocity to the rate of increasing width of the growth face, the computer simulation produced curved crystals of truncated lozenge or lenticular shape, both of which have been observed experimentally. The change in morphology has been analysed quantitatively. Copyright © 1996 Elsevier Science Ltd.

**(Keywords: computer simulation; anisotropic growth condition; curved crystal habit)**

## INTRODUCTION

Single crystals of polyethylene with curved lateral habit have been reported by several researchers[1–3] in their work on crystallization from dilute solutions. The crystals are basically truncated lozenges with curved edges on the {100} growth faces (type B in *Figure 1b*). Single crystals of lenticular shape (type A in *Figure 1a*) have also been reported when polyethylene is crystallized from the melt or from solutions at higher temperatures (e.g. 106°C)[1,4,5]. Furthermore, in the case of crystallization from the melt, polyethylene single crystals show a morphological change from type A to type B which accompanies the transition in growth regime from I to II[6–8]. To understand the formation mechanism of these curved crystals is one of the current problems in this field. In the earliest approach proposed by Sadler[9], thermal roughening of the growth face was responsible for the curved crystals, but the idea was incompatible with the standard models of polymer crystallization[10] in which the limiting process is surface nucleation, a process unnecessary for the growth of thermally roughened faces. Toda[11] proposed an alternative approach, introducing some interruption effect on the step propagation on the basis of nucleation-controlled growth. Such an interruption effect is also able to cause curved growth edges, as typically seen in the impurity effect on the crystal habits of simple molecules[12].

Following the second approach, Mansfield[13] proposed a theoretical model which allowed us to study the morphological change in more detail. The approach is based on a model proposed by Seto[14] and Frank[15] and takes the effect of substrate growth into account by introducing a moving boundary condition. Mansfield's model successfully produced the curved growth front of type B crystals of polyethylene (*Figure 1b*) for the spreading rate of substrate $h$ being comparable with the propagation velocity of steps $v$, of $h \lesssim v$; the profile of the growth front is represented by an arc of an ellipse in the asymptotic form. Toda[5] extended the model for the case of substrate spreading faster than the propagation of steps, $h > v$, and showed that the lenticular profile (type A in *Figure 1a*) is also predicted from the model. Point and Villers[16] obtained the numerical solutions of a differential equation derived from the model of Seto and Frank with a moving boundary condition; the resultant crystals were also type A and type B. In these models, an unusually slow propagation of steps is essential to produce the curved growth front. The origin of such a slow propagation of steps has not been identified; possible candidates are impurities[11], self-poisoning[17], lattice strain[18] and domain boundaries[8].

All the above approaches are based on the model of Seto and Frank, describing nucleation and growth processes on a continuous one-dimensional substrate, and hence the approaches should be considered as an idealization of the real crystals formed on a discrete lattice. Strictly speaking, the detailed analyses of the models are applicable only to growth with a sufficiently

* To whom correspondence should be addressed
† Current address: Faculty of Integrated Arts and Sciences, Hiroshima University, Higasi-Hiroshima 739, Japan

low step density. In dealing with the curved lateral habits of actual crystals, however, we always encounter the situation of extremely high step density, which is solely responsible for the curved profile of the growth front. In order to do a detailed inspection of the curved profile and its growth kinetics, we must perform a computer simulation of a discrete lattice.

In this work, we perform a Monte Carlo simulation of a two-dimensional hexagonal lattice, applying an anisotropic growth condition to model polyethylene crystallization into an orthorhombic cell. Here 'hexagonal lattice' only means that each site has six nearest neighbours and we assign the indices [100] and [010] to two orthogonally crossed directions according to the lattice of polyethylene crystals. A large difference in the growth rates of the {110} and {100} faces is essential to produce the curved crystals of type A and type B.

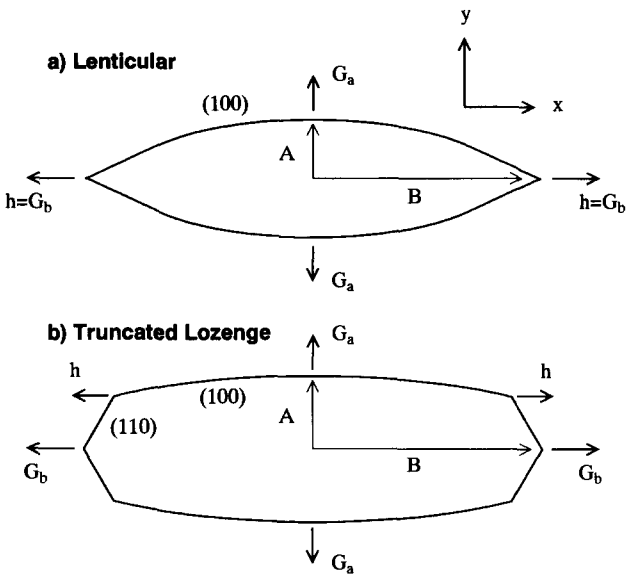


**Figure 1** Schematic illustration of (a) a lenticular shape (type A) and (b) a truncated lozenge with curved edges (type B). Both types are composed of {100} and {110} growth sectors. The width of the {110} sectors in the type A crystal is too narrow to be recognized

## MODEL

We treat the growth of two-dimensional crystals on a hexagonal lattice; the crystallization unit is called a 'stem'. The scale factors are the stem width $a$ and the stem height $b$ (*Figure 2*). In the simulation, a crystal grows through two processes: one is nucleation and the other is step propagation. The probabilities of these processes are denoted as $ia$ and $v/a$, respectively, because of the dimensions of the rate $i$ ($cm^{-1}s^{-1}$) and the velocity $v$ ($cm\,s^{-1}$). These two processes are performed successively in the time sequences, as follows. Firstly, the number of nucleation events $n_i$ is determined from a Poisson distribution. Let the number of flat sites be $N$, then the average number of nucleation events $\langle n_i \rangle$ is $Nia$, and the probability $p(n_i)$ becomes

$$p(n_i) = \frac{\langle n_i \rangle^{n_i}}{n_i!}\exp(-\langle n_i \rangle) = \frac{(Nia)^{n_i}}{n_i!}\exp(-Nia)$$

According to the probability, the number of nucleation events is determined by a random number $r$ ($0 \leq r \leq 1$). If the random number $r$ satisfies the condition

$$\sum_{i=0}^{n_i} p(i) \leq r < \sum_{i=0}^{n_i+1} p(i)$$

then the number of nucleation events is determined as $n_i$. The positions of these nuclei are selected using a random number generated separately. This procedure is of advantage for reducing the execution time of the simulation, but only when $ia$ is small enough[19]. Secondly, for the step propagation, each niche site is examined to determine whether the step has advanced forwards or not. Each computer simulation is continued until the

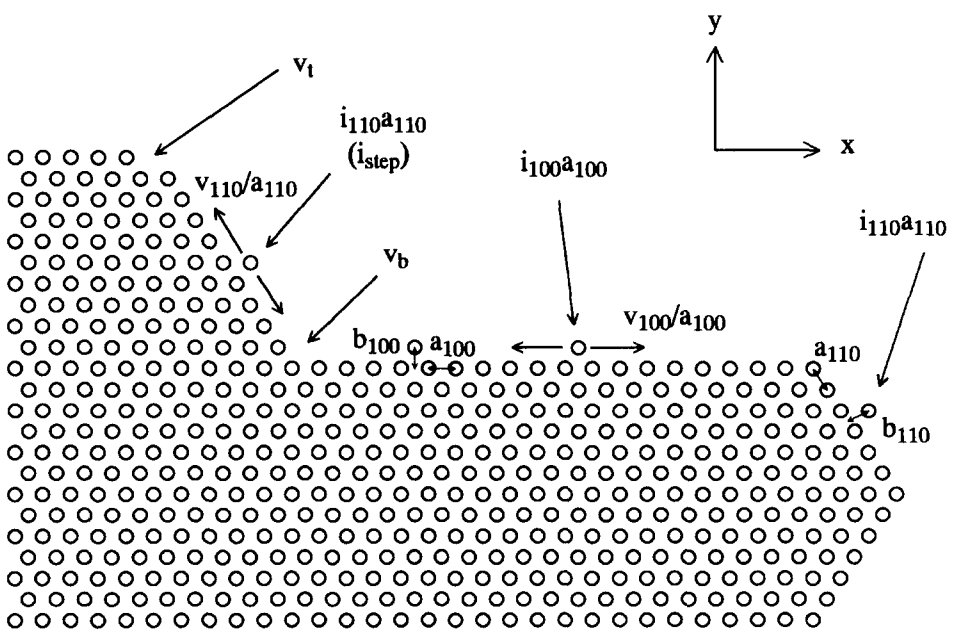


**Figure 2** Schematic illustration of the growth front and definition of the parameters used in the simulation. The $b$ axis is horizontal and the $a$ axis vertical

system reaches a steady state (until the growth rates $G_a$ and $G_b$ become constant); the crystal size is at least 5000 lattice sites.

In order to introduce an anisotropic growth condition, we give $ia$ and $v/a$ two values according to the {110} and {100} growth faces. To distinguish the rates on these growth faces, we denote the rates as $i_{100}a_{100}$, $i_{110}a_{110}$, $v_{100}/a_{100}$ and $v_{110}/a_{110}$. To complete the step propagation at the edges of multilayer steps and the {110} and {100} growth sectors, we must distinguish the two additional situations of the attachment of a new stem to the bottom corner and to the top corner of a multilayer step or the edges of a growth sector, and consequently we need to introduce the probabilities $v_b$ and $v_t$ of the respective processes (*Figure 2*). Here, we need to settle the complex conditions for the deposition rate at the corners; however, this is beyond our knowledge available from the experimental results. At present, we simply choose to put $v_b = v_{100}/a_{100}$ in the simulation because our main concern is the growth on the {100} faces. The choice of $v_t$ is more complicated because this parameter controls the stability of multilayer steps; a slow filling rate of $v_t$ causes the decomposition of multilayer steps. In the simulation, we examine two cases: $v_t = v_{100}/a_{100}$ and $v_t = v_{110}/a_{110}$.

In our model, the six parameters detailed above determine the growth kinetics and the morphology of a two-dimensional crystal formed on an orthorhombic lattice. The rate of increasing width of the growth substrate $h$ is automatically determined by these parameters because the simulation is of a two-dimensional crystal. From the number of controlling parameters, it seems that there might be an extremely wide choice of parameters. However, since we are concerned with the conditions generating type A and type B crystals, we require that (1) the aspect ratio $B/A$ be less than around 3, (2) $h_{100}$ be approximately equal to $v_{100}$ and (3) the step density on the {110} face be low enough so that the facets of the {110} growth faces can be observed. According to the first condition, we set $i_{100}a_{100}^2/v_{100} = 1/30$ for the aspect ratio of 2.6 obtained from lenticular crystals experimentally[5,6,8]. From the second condition, we set $v_{100} \approx b_{110}i_{110}L_{110}$ ($\approx h_{100}$), expecting single-nucleation growth of the {110} growth face in lenticular crystals. Finally, from the third condition, we set $i_{110}a_{110}^2/v_{110} \ll 1$. Taking these conditions into account, we set $i_{100}a_{100} = 10^{-3}$ and $v_{100}/a_{100} = 0.03$, and the probability of the fastest process, namely $v_{110}/a_{110}$, is always set at 1. To control the value of $h_{100}/v_{100}$ in our simulation, we choose $i_{110}a_{110}$ as the controlling parameter because of the advantage in comparing results and the ease with which we can change the value; if we choose $v_{100}/a_{100}$, we will have to change other parameters simultaneously. The value of $i_{110}a_{110}$ is chosen from the range $10^{-4}$–$6 \times 10^{-3}$. Additionally, to make a clear comparison between simulation and theoretical results, we also adopt the condition $i_{110}a_{100}^2/v_{100} = 1/300$ for the case of low step density. The remaining two parameters $v_b$ and $v_t$ are determined as stated above. The parameters used in the simulation are listed in *Table 1*, as are the results for $h_{100}/v'_{100}$ (where $v'_{100}$ is a corrected step propagation rate defined later), the aspect ratio $B/A$ and crystal type.

In our model, we neglect the probability of the detachment of stems. But this does not mean that we simply ignore the fluctuation of step propagation; fluctuation can be introduced by making the probability $v_{100}a_{100}$ less than 1. In general, detachment processes will not be important unless the difference between the rates of attachment and detachment is small enough, and this is the case under the usual conditions of polymer crystallization.

## THEORETICAL

In this section, we refer to the results of the theoretical calculations of Mansfield[13] ($h < v$) and Toda[5] ($h > v$). Since we are concerned with the curved growth front of the {100} growth face, all the subscripts which specify the {100} growth face are omitted in this section.

The basis of these calculations is a couple of differential equations suggested by Seto[14] and Frank[15]. The equations describe the change in the densities of left-moving and right-moving steps, $l(x,t)$ and $r(x,t)$, at a position $x$ and time $t$ on a one-dimensional substrate of length $L$. The growth rate $G$ and the profile of the growth front are given by $G = b(l+r)v (\equiv 2bcv$, where $2c$ is the total step density) and by the integration of $b(l-r)$, respectively[15]. Employing the moving boundary condition $L = 2ht$, Mansfield[13] obtained an asymptotic solution of the differential equations for $h < v$

$$\left.\begin{aligned} r(x,t) &\approx \left[\left(\frac{i}{2v}\right)\left(\frac{vt+x}{vt-x}\right)\right]^{1/2} \\ l(x,t) &\approx \left[\left(\frac{i}{2v}\right)\left(\frac{vt-x}{vt+x}\right)\right]^{1/2} \end{aligned}\right\} (0 \le |x| \le ht) \qquad (1)$$

These step densities give the profile of the growth front as

$$y = Gt[1 - (x/vt)^2]^{1/2} \qquad (2)$$

where $x$ and $y$ are the coordinates of the [010] and [100] directions in *Figure 1*, respectively. Equation (2) represents an ellipse, the shape of which is independent of the rate $h$. The substrate spreading rate $h$ determines the positions of the edges of the growth substrate, $x = \pm ht$, in the ellipse. Since the solution gives a six-sectored single crystal composed of two {100} growth sectors and four well-developed {110} sectors, we call this profile a 'truncated lozenge' with curved edges (type B in *Figure 1b*).

In the case of $h > v$, the densities of right-moving and left-moving steps are given in the positive $x$ region by[5]

$$\left.\begin{aligned} r(x,t) &\approx \left[\left(\frac{i}{2v}\right)\left(\frac{vt+x}{vt-x}\right)\right]^{1/2} \\ l(x,t) &\approx \left[\left(\frac{i}{2v}\right)\left(\frac{vt-x}{vt+x}\right)\right]^{1/2} \end{aligned}\right\} \left(0 \le x \le \frac{v^2}{h}t\right) \qquad (3)$$

$$\left.\begin{aligned} r(x,t) &\approx \left[\left(\frac{i}{2v}\right)\left(\frac{h+v}{h-v}\right)\right]^{1/2} \\ l(x,t) &\approx \left[\left(\frac{i}{2v}\right)\left(\frac{h-v}{h+v}\right)\right]^{1/2} \end{aligned}\right\} \left(\frac{v^2}{h}t \le x < ht\right) \qquad (4)$$

For negative $x$, the symmetry relation $r(-x,t) = l(x,t)$ holds. It should be noted that in the vicinity of $x = \pm ht$, equations (4) are not the exact solution because of the boundary condition $l(\pm ht, t) = r(\pm ht, t) = 0$. A characteristic of the solution is the constant step densities

near the edges of the substrate, i.e. ($v^2t/h \leq |x| < ht$, as seen in equations (4). This means that the profile becomes linear near the edges, while the central region (equations (3)) is represented by Mansfield's ellipse of equation (2). Since the substrate spreads faster than the propagation of steps, the substrate does not grow at the edges, $x = \pm ht$, and consequently the width of the {110} growth sectors is kept constant from the early stages of growth; the lateral habit expected from this solution is a 'lenticular shape' (type A in *Figure 1a*).

## RESULTS AND DISCUSSION

### *Profile*

*Figure 3* shows the lateral habits and the morphological change obtained in the present simulation for $i_{100}a_{100}^2/v_{100} = 1/30$ and $v_t = v_{100}/a_{100}$. It is clear that depending on the value of $h_{100}/v'_{100}$ or $i_{110}a_{110}$, the crystals change habit from truncated lozenge (type B) to lenticular shape (type A). In the type A crystals in *Figures 3e* and *3f*, the width of the {110} growth sectors was kept constant from the early stages of growth. The width was several tens of sites and the {110} sectors cannot be seen in the figures at the given magnifications.

The morphological change seen in the simulation agrees with the theoretical predictions described above[5,6,8]. In quantitative comparison with the theoretical calculations, however, the results of simulation do not agree well with the calculations. The discrepancies between the theoretical calculations and the simulation results will be discussed below in detail. Here, it should be noted that the morphological change from type B does not occur at $h_{100}/v'_{100} = 1$, in contrast to the theoretical prediction[5,6,8]. The value of $h_{100}/v'_{100}$ needs to be somewhat larger than 1 to give rise to the transition. This is because the growth in width of the {110} sectors is enabled by nucleation at the outermost edges of the {100} growth face, in spite of the condition $h_{100}/v'_{100} \geq 1$. Additionally, the choice of $v_t$ also affects the resultant morphology; a smaller $v_t$ brings a decrease in the growth rate of the width and vice versa. Such an effect of $v_t$ can be seen in simulations 1–9 in *Table 1*. By the choice of $v_t = v_{110}/a_{110}$, the width of the {110} sectors is kept constant only for simulation 9 with the quite large values $h_{100}/v'_{100} = 2.80$ and $B/A = 9.8$. We are not able to judge whether the choice of $v_t = v_{100}a_{100}$ in the present simulation is a realistic one or not. At least it is certain that the process of filling in at the corners is one of the

**Table 1** Parameters used in the simulation and the results for $h_{100}/v'_{100}$, aspect ratio $B/A$ and crystal type. The other fixed parameters are $v_{100}/a_{100} = v_b = 0.03$ and $v_{110}/a_{110} = 1$

| Simulation | $i_{100}a_{100}^2/v_{100}$ | $v_t$ | $i_{110}a_{110}$ | $h_{100}/v'_{100}$ | $B/A$ | Type |
|---|---|---|---|---|---|---|
| 1 | 1/30 | $v_{110}/a_{110}$ | $10^{-5}$ | 0.01 | 0.54 | B |
| 2 | | | $6 \times 10^{-5}$ | 0.23 | 1.3 | B |
| 3 | | | $10^{-4}$ | 0.33 | 1.7 | B |
| 4 | | | $3 \times 10^{-4}$ | 0.68 | 2.8 | B |
| 5 | | | $6 \times 10^{-4}$ | 1.02 | 3.9 | B |
| 6 | | | $10^{-3}$ | 1.36 | 5.1 | B |
| 7 | | | $2 \times 10^{-3}$ | 1.85 | 6.9 | B |
| 8 | | | $3 \times 10^{-3}$ | 2.22 | 8.1 | B |
| 9 | | | $6 \times 10^{-3}$ | 2.80 | 9.8 | A |
| 10 | | $v_{100}/a_{100}$ | $2 \times 10^{-4}$ | 0.68 | 2.6 | B |
| 11 | | | $3 \times 10^{-4}$ | 0.87 | 3.1 | B |
| 12 | | | $4 \times 10^{-4}$ | 1.03 | 3.5 | B |
| 13 | | | $6 \times 10^{-4}$ | 1.27 | 4.3 | B |
| 14 | | | $10^{-3}$ | 1.40 | 4.8 | A |
| 15 | | | $1.5 \times 10^{-3}$ | 1.45 | 5.0 | A |
| 16 | | | $3 \times 10^{-3}$ | 1.53 | 5.3 | A |
| 17 | | | $6 \times 10^{-3}$ | 1.65 | 5.6 | A |
| 18 | 1/300 | $v_{110}/a_{110}$ | $5 \times 10^{-6}$ | 0.05 | 1.0 | B |
| 19 | | | $10^{-5}$ | 0.10 | 1.5 | B |
| 20 | | | $10^{-4}$ | 0.41 | 5.1 | B |
| 21 | | | $3 \times 10^{-4}$ | 0.72 | 8.3 | B |
| 22 | | | $4 \times 10^{-4}$ | 0.86 | 9.6 | B |
| 23 | | | $5 \times 10^{-4}$ | 0.96 | 11 | B |
| 24 | | | $5.5 \times 10^{-4}$ | 1.02 | 12 | B |
| 25 | | | $6 \times 10^{-4}$ | 1.06 | 12 | B |
| 26 | | | $10^{-3}$ | 1.29 | 15 | B |
| 27 | | | $3 \times 10^{-3}$ | 1.74 | 20 | A |
| 28 | 1/300 ($i_{step} = 0$) | $v_{110}/a_{110}$ | $6 \times 10^{-4}$ | 1.01 | 11 | B |
| 29 | | | $7 \times 10^{-4}$ | 1.03 | 12 | A |
| 30 | | | $10^{-3}$ | 1.12 | 13 | A |
| 31 | | | $2 \times 10^{-3}$ | 1.30 | 15 | A |

most important factors determining the lateral habits in the actual crystallization process.

*Growth rate of the {100} face*

Before starting the discussion, we need to introduce two different step densities. One is $c^{(s)}$ and the other $c^{(m)}$; a multilayer step is counted once as a single step in the former density, and in the latter it is counted according to the number of layers in the step. The former density represents that of number-averaged steps and the latter that of weight-averaged steps. In the evaluation of growth rate and slope, we need to use $c^{(m)}$.

The growth rate $G_a$ is determined by the growth kinetics in the central region of the {100} growth face. On such a well-developed growth face as that of the {100} sector, it is reasonable to assume multinucleation growth. The growth rate in this mode is usually represented by

$$G_a = b_{100}(2i_{100}v_{100})^{1/2} \tag{5}$$

For growth on a discrete lattice, however, we must consider the following two additional effects, especially under the condition of high step density encountered in the simulation. Firstly, nucleation at a niche site on a discrete lattice has no physical meaning, and hence these niche sites must be ruled out as sites for nucleation. The average nucleation rate $i'_{100}(x)$, taking account of this effect is represented by

$$i'_{100}(x) = i_{100}\left[1 - 2c^{(s)}_{100}(x)\right] \tag{6}$$

Since we are concerned with the growth kinetics around the centre, we use the step density and the nucleation rate at $x = 0$. Secondly, in the expression of equation (5) we have not counted the contribution of the nucleus itself to the growth rate. On including these effects in the growth rate, we can write the modified growth rate $G_a^{(\mathrm{calc})}$ as

$$G_a^{(\mathrm{calc})} = b_{100}\left[i'_{100}a_{100} + \left(2i'_{100}v_{100}\right)^{1/2}\right] \tag{7}$$

In *Table 2* are listed the simulation results for growth rate $G_a/b$ step density $2c^{(s)}_{100}(0)a$, the calculated growth rate $G_a^{(\mathrm{calc})}/b$ and the ratio of the growth rates $G_a/G_a^{(\mathrm{calc})}$ for the cases $v_t = v_{110}/a_{110}$ and $v_t = v_{100}/a_{100}$. It can be seen that for $v_t = v_{110}/a_{110}$, $G_a$ and $G_a^{(\mathrm{calc})}$ are in good agreement with each other within 1% (simulations 2–9). This indicates that the continuous model is a good approximation for the growth rate around the centre in spite of the high step density. On the other hand, for $v_t = v_{100}/a_{100}$, $G_a$ becomes smaller than $G_a^{(\mathrm{calc})}$ by about 10% (simulations 10–17). The discrepancy can be explained as the result of a special manner of propagation of multilayer steps on the discrete lattice with $v_t = v_{100}/a_{100}$, because multilayer steps are unstable for $v_t = v_{100}/a_{100}$, as mentioned earlier. We can expect a decrease in the average velocity of step propagation $v_{100}$ because of this effect. Assuming that

$$G_a^{(\mathrm{sim})} = b_{100}\left[i'_{100}a_{100} + \left(2i'_{100}v'_{100}\right)^{1/2}\right] \tag{8}$$

the corrected step propagation rate $v'_{100}$ can be evaluated from equations (7) and (8), giving

$$v'_{100}/a_{100} = (v_{100}/a_{100})\left(\frac{G_a^{(\mathrm{sim})}/b_{100} - i'_{100}a_{100}}{G_a^{(\mathrm{calc})}/b_{100} - i'_{100}a_{100}}\right)^2 \tag{9}$$

The corrected values are also tabulated in *Table 2*.

Except for $i_{100}a_{100}^2/v_{100} = 1/30$ and $v_t = v_{100}/a_{100}$, the difference between $v_{100}$ and $v'_{100}$ is negligible because $G_a^{(\mathrm{calc})}$ and $G_a^{(\mathrm{sim})}$ are in good agreement. In addition, the step densities are so low that no correction in nucleation rate is needed for $i_{100}a_{100}^2/v_{100} = 1/300$.

*Step densities*

Since the solutions of the analytical models are given in the form of step densities $l$ and $r$, we can make a straightforward comparison between the step densities obtained from the simulation and the theoretical predictions. The simulation results are plotted in *Figures 4–7*; the horizontal axis in each figure is scaled with $v'_{100}t$.

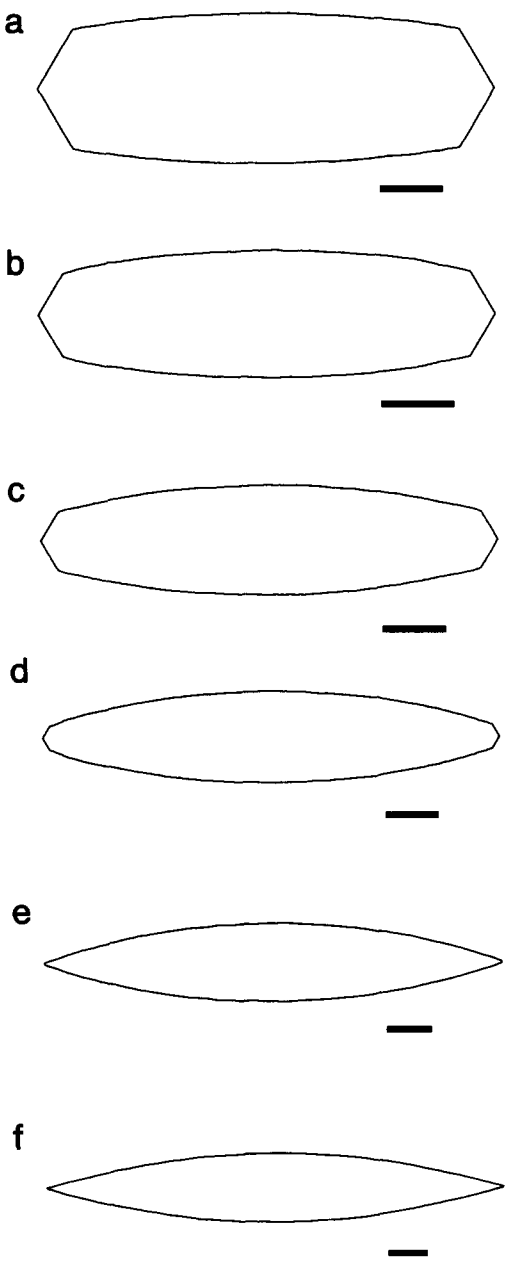


**Figure 3** Two-dimensional crystals created by the simulation. The results are for simulations 10 (a), 11 (b), 12 (c), 13 (d), 15 (e) and 17 (f) from *Table 1*. The bar corresponds to a width of 1000 sites

**Table 2** Lists of growth rates for $i_{100}a_{100}^2/v_{100} = 1/30$ and $v_{100}/a_{100} = 0.03$; $(2i_{100}v_{100})^{1/2} = 0.00775$. The other parameters used in each simulation are those assigned the same simulation number as shown in *Table 1*

| Simulation | $v_t$ | $G_a/b$ | $2c_{100}^{(s)}(0)a$ | $G_a^{(calc)}/b$ | $G_a/G_a^{(calc)}$ | $v'_{100}/a_{100}$ |
|---|---|---|---|---|---|---|
| 2 | $v_{110}/a_{110}$ | 0.00767 | 0.19 | 0.00778 | 0.99 | $v_{100}/a_{100}$ |
| 3 | | 0.00772 | 0.18 | 0.00783 | 0.99 | |
| 4 | | 0.00770 | 0.18 | 0.00783 | 0.98 | |
| 5 | | 0.00791 | 0.19 | 0.00778 | 1.01 | |
| 6 | | 0.00779 | 0.20 | 0.00773 | 1.01 | |
| 7 | | 0.00779 | 0.18 | 0.00783 | 0.99 | |
| 8 | | 0.00808 | 0.17 | 0.00789 | 1.02 | |
| 9 | | 0.00828 | 0.19 | 0.00778 | 1.06 | |
| 10 | $v_{100}/a_{100}$ | 0.00685 | 0.21 | 0.00767 | 0.89 | 0.023 |
| 11 | | 0.00693 | 0.22 | 0.00762 | 0.91 | 0.024 |
| 12 | | 0.00682 | 0.23 | 0.00757 | 0.90 | 0.024 |
| 13 | | 0.00685 | 0.23 | 0.00757 | 0.91 | 0.024 |
| 14 | | 0.00675 | 0.22 | 0.00762 | 0.89 | 0.023 |
| 15 | | 0.00698 | 0.22 | 0.00762 | 0.92 | 0.025 |
| 16 | | 0.00695 | 0.22 | 0.00762 | 0.91 | 0.024 |
| 17 | | 0.00697 | 0.22 | 0.00762 | 0.91 | 0.025 |

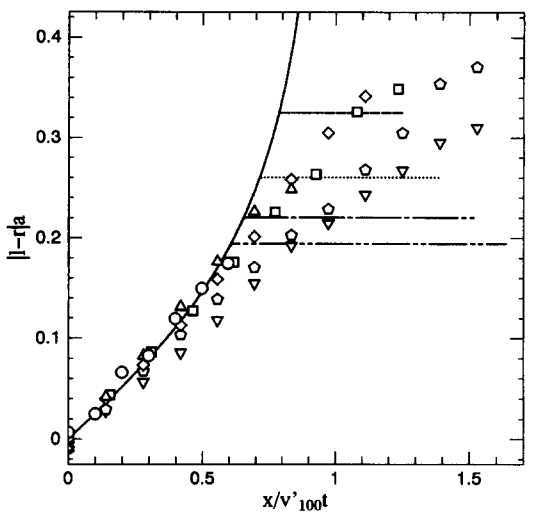


**Figure 4** Profile slopes $|l - r|a$ plotted against $|x/v'_{100}t|$. The plots are for simulations 10 (○), 12 (△), 13 (◇), 14 (□), 16 (⌓) and 17 (▽) from *Table 1*. The theoretical curves are calculated with $i'a = 7.8 \times 10^{-4}$ and $v'/a = 0.024$: (——) Mansfield's ellipse; (– – –) $h_{100}/v'_{100} = 1.27$; (· · · · · ·) $h_{100}/v'_{100} = 1.40$; (-· · · · · ·-) $h_{100}/v'_{100} = 1.53$; (-· · · · · ·-) $h_{100}/v'_{100} = 1.65$

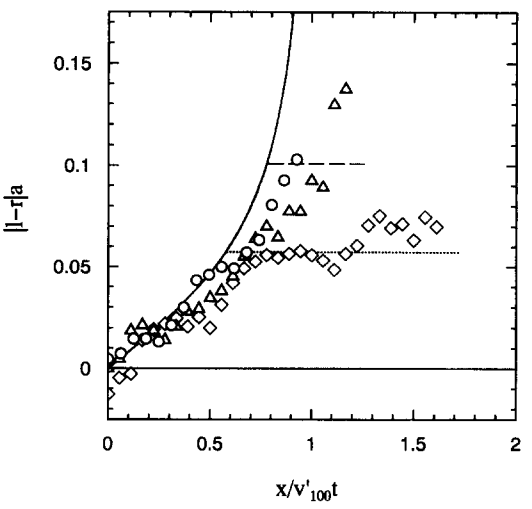


**Figure 5** Profile slopes $|l - r|a$ plotted against $|x/v'_{100}t|$. The plots are for simulations 25 (○), 26 (△) and 27 (◇) from *Table 1*. The theoretical curves are calculated with no correction for $ia$ and $v/a$: (——) Mansfield's ellipse; (– – –) $h_{100}/v'_{100} = 1.29$; (· · · · · ·) $h_{100}/v'_{100} = 1.74$

The step densities are calculated for each 500 sites and the moving average method is used as a smoothing technique: the sum of three adjoined data is divided by 3 and the resulting value is plotted as a value at the centre of the three data. The step densities around the edges are not shown in these figures because in the vicinity of the edges of the growth face, it becomes difficult to locate the boundaries between the {100} and {110} growth sectors owing to the formation of multilayer steps. It should also be noted that the corrected values of $i_{100}a_{100}$ and $v_{100}/a_{100}$ defined as above are used for the calculation of the theoretical curves.

*Figures 4* and *5* are the plots of the profile slopes $|l - r|a$ obtained under several growth conditions listed in *Table 1*; *Figure 4* applies to a high step density, while *Figure 5* applies to a low step density. *Figure 6* shows the average step densities $2c^{(s)}a$ and $2c^{(m)}a$ for the same conditions as in *Figure 4*.

The plots of simulations 10, 12 and 13 in *Figure 4* and simulations 25 and 26 in *Figure 5* are of truncated lozenge shape (type B), and the plots of simulations 16 and 17 in *Figure 4* and simulation 27 in *Figure 5* are of lenticular shape (type A) (see *Figure 3*). It can be seen that the plots of truncated lozenge shape are on a single master curve, though the curve gradually deviates from Mansfield's ellipse with increasing $x/v'_{100}t$. Concerning the slope of lenticular shape in contrast to the theoretical prediction of a constant slope near the edges, a monotonous increase is seen in the slopes of simulations 16 and 17 in *Figure 4*, while the slope of simulation 27 in *Figure 5* gradually levels off near the edge. On the other hand, in *Figure 6* the plots of $2c^{(m)}a$ should be compared with the theoretical curves in the figure. We can see the

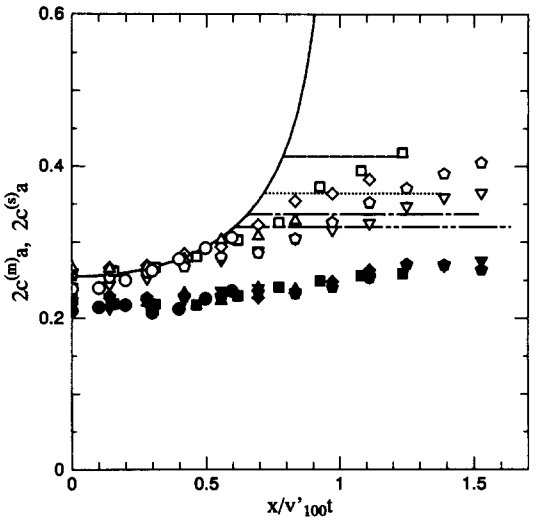


**Figure 6** Average step densities $2c^{(s)}a$ and $2c^{(m)}a$ plotted against $|x/v'_{100}t|$. The plots are for simulations 10 (○), 12 (△), 13 (◇), 14 (□), 16 (⌂) and 17 (▽) from *Table 1*. The open symbols are for $c^{(m)}$, the closed symbols for $c^{(s)}$. The theoretical curves are calculated with $i'a = 7.8 \times 10^{-4}$ and $v'/a = 0.024$: (——) Mansfield's ellipse; (– – –) $h_{100}/v'_{100} = 1.27$; (·····) $h_{100}/v'_{100} = 1.40$; (-·-·-·-) $h_{100}/v'_{100} = 1.53$; (-···-) $h_{100}/v'_{100} = 1.65$

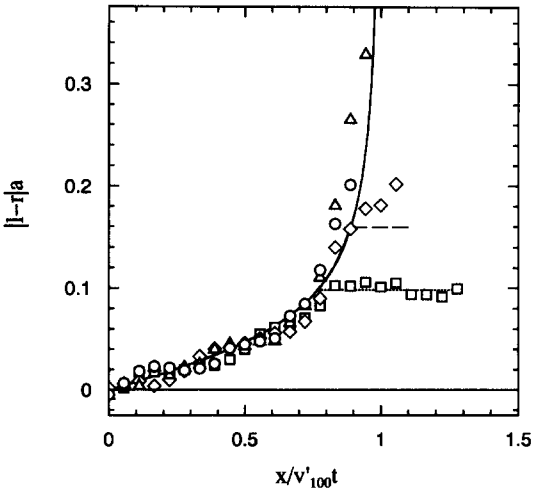


**Figure 7** Plots of profile slopes $|l - r|a$ with the additional restriction of $i_{step} = 0$. The plots are for simulations 28 (○), 29 (△), 30 (◇) and 31 (□) from *Table 1*. The theoretical curves are calculated with no correction for $ia$ and $v/a$: (——) Mansfield's ellipse; (– – –) $h_{100}/v'_{100} = 1.12$; (·····) $h_{100}/v'_{100} = 1.30$

discrepancies between them in the same manner as in *Figures 4* and *5*.

From *Figure 6*, it can also be seen that the value of $2c^{(s)}a$ shows a weaker dependence on $x/v'_{100}t$ than $2c^{(m)}a$. We can regard the ratio between these step densities as an average step height. This means that the average height of multilayer steps increases with $x/v'_{100}t$, and the contribution of multilayer steps to the growth becomes larger near the edges of the {100} growth face than at the centre of it. This fact gives us an important clue to help us clarify the origin of the discrepancies. In our model, we did not inhibit nucleation on the side surfaces of multilayer steps. The effects of these nucleations can be examined by carrying out simulations under the condition of low step density, i.e. $i_{100}a^2_{100}/v'_{100} = 1/300$ and $v_t = v_{110}/a_{110}$, with an additional restriction that the nucleation events on the side surfaces of multilayer steps are inhibited on the {100} growth face; the growth conditions (simulations 28–31) are listed in *Table 1*. The results in *Figure 7* show that the plots agree well with the theoretical curves even for a lenticular shape. From this fact, we can conclude that the discrepancy between the simulation and theoretical results is mainly due to the nucleation events on the side surfaces of multilayer steps.

## CONCLUSIONS

Our Monte Carlo simulation reproduced lateral habits of truncated lozenge and lenticular shape, as exhibited by polyethylene single crystals. Comparison with the profiles calculated theoretically, however, gave less agreement. The discrepancies are due to the discreteness of the actual crystal lattice, since the theoretical models assume a continuous substrate. Among all the possible effects of this discreteness, it is concluded that nucleation on the side surfaces of multilayer steps has a great influence on the profile of the growth front. The choice of the filling rate at the top and bottom corners of the multilayer step is also not trivial; the profile and the growth rate can be significantly affected by this choice. It is not an easy task to introduce the effects into any analytical treatment, and hence the simulational approach has its own significance. To investigate the microscopic mechanism of creating curved edges, namely of slow step propagation on the {100} growth face, we certainly need a simulational method for a discrete lattice.

## ACKNOWLEDGEMENTS

We would like to thank Professors Y. Ohde and M. Sugiyama (NIT), Professor H. Miyaji and Dr K. Izumi (Kyoto University), and Professor M. Hikosaka (Hiroshima University) for their valuable discussions and encouragement. We are grateful to Mr K. Motosita (NIT) for his technical support in this work.

## REFERENCES

1 Takamizawa, K., Urabe, Y. and Hara, T. *Rep. Prog. Polym. Phys. Jpn. 1969*, **10**, 163
2 Khoury, F. *Faraday Discuss. Chem. Soc.* 1979, **68**, 404
3 Organ, S. J. and Keller, A. *J. Mater. Sci.* 1985, **20**, 1571
4 Bassett, D. C., Olley, R. H. and Al Raheil, I. A. M. *Polymer* 1988, **29**, 1539
5 Toda, A. *Polymer* 1991, **32**, 771
6 Toda, A. *Colloid Polym. Sci.* 1992, **270**, 667
7 Toda, A. and Keller, A. *Colloid Polym. Sci.* 1993, **271**, 328
8 Toda, A. *Faraday Discuss. Chem. Soc.* 1993, **95**, 129
9 Sadler, D. M. *Polymer* 1983, **24**, 1401
10 Hoffman, J. D., Davis, G. T. and Lauritzen Jr, J. I. in 'Treatise on Solid State Chemistry' (Ed. J. B. Hannay), Vol. 3, Plenum Press, New York, 1976, Ch. 7
11 Toda, A. *J. Phys. Soc. Jpn* 1986, **55**, 3419
12 Black, S. N., Bromley, L. A., Cottier, D., Davey, R. J., Dobbs, B. and Rout, J. E. *J. Chem. Soc. Faraday Trans.* 1991, **87**, 3409
13 Mansfield, M. L. *Polymer* 1988, **29**, 1755
14 Seto, T. *Rep. Prog. Polym. Phys. Jpn* 1964, **7**, 67
15 Frank, F. C. *J. Cryst. Growth* 1974, **22**, 233
16 Point, J.-J. and Villers, D. *J. Cryst. Growth* 1991, **114**, 228
17 Ungar, G. and Keller, A. *Polymer* 1987, **28**, 1899
18 Hoffman, J. D. and Miller, R. I. *Macromolecules* 1989,. **22**, 3038
19 Toda, A. and Tanzawa, Y. *J. Cryst. Growth* 1986, **76**, 462